Received: 21 December 2018 | Revised: 5 March 2019 | Accepted: 2 April 2019

DOI: 10.1002/pip.3143

RESEARCH ARTICLE

WILEY PROGRESS IN PHOTOVOLTAICS

Transient carrier recombination dynamics in potential-induced degradation p-type single-crystalline Si photovoltaic modules

Mohammad Aminul Islam[1] | Hiroyuki Matsuzaki[2] | Yuusuke Okabayashi[2] | Yasuaki Ishikawa[1]

[1] Division of Materials Science, Nara Institute of Science and Technology, Ikoma, Nara 630-0192, Japan

[2] Research Institute for Measurement and Analytical Instrumentation, National Institute of Advanced Industrial Science and Technology, Tsukuba, Ibaraki 305-8568, Japan

Correspondence
Mohammad Aminul Islam and Yasuaki Ishikawa, Nara Institute of Science and Technology, Ikoma, Nara 630-0192, Japan.
Email: aminbgm@gmail.com; yishikawa@ms.naist.jp

Funding information
New Energy and Industrial Technology Development Organization (NEDO), Japan

Abstract

In this study, we investigated the recombination dynamics of minority carriers through the decay profile analysis of transient diffuse reflectance spectroscopy (TDRS) for fresh and potential-induced degradation (PID) modules. The PID-affected region in terms of the degradation degree on the modules was firstly localized using conventional methods such as electroluminescence (EL) and lock-in thermal images. The photogenerated carrier density and carrier lifetime were different in photovoltaic (PV) modules in fresh and PID modes. It was found that the dominant recombination involved the carrier transition via shallow trap states. The distribution of the trap states, however, was extended from the surface to the bulk of the solar cell due to Na ions–decorated defects. The behaviors of the carrier dynamics near the surface and bulk were very different, as inferred from the two different pump wavelengths of 532 and 1064 nm, respectively.

KEYWORDS

carrier lifetime, crystalline Si, potential-induced degradation, recombination, shallow defect, transient diffuse reflectance spectroscopy

1 | INTRODUCTION

Potential-induced degradation (PID) has recently attracted considerable attention owing to its significant negative impact on the performance of photovoltaic (PV) systems.[1] It is considered that massive power losses in megawatt PV systems are related to the strong detrimental impact of PID.[2] Associated with the higher potential distress originating in PV systems, PID is distinctly different from other causes of module efficiency deterioration.[3] Na ions arise and migrate from soda-lime glass that is used as a cover on the modules. Shunt and leakage current are influenced by the Na ions that have been ascribed as a principal cause of PID.[2-5] PID at the cell and module level depends on the encapsulation materials and/or the composition of silicon nitride (SiN_x) as an antireflection coating on PV cells. Although some procedures for preventing PID are performed at the cell, module, and system level through macroscopic analyses, some technologies are already partly applied in production[6] to suppress PID, such as characterization by electroluminescence (EL), lock-in thermography (LIT), and current-voltage (*I-V*) measurement techniques. However, the origin of PID at the microscopic scale is not yet clear.

Additionally, the performances of solar cell devices or *I-V* characteristics are just the final results of a series of fundamental processes, including photon absorption, charge generation and recombination, and charge collection in solar cells. Charge generation occurs under photoexcitation and is an important requirement for high-performance solar cells that utilize these photogenerated carriers before recombination. Thus, we expect a crucial difference in the charge carrier generation and collection between PID-affected and unaffected silicon-based solar cells. Free electrons and holes are immediately generated upon photoexcitation in Si solar cells. The number of carriers and their mobility, however, are highly affected by PID. The Na ions that reach the Si surface can increase the defect states on the surface or penetrate through stacking faults, leading to the recombination of free carriers and/or their entrapment in these defect

states. Consequently, free carriers that can reach the interface before recovery to the ground state are significantly lower in PID-affected solar cells, and the power conversion efficiency is degraded. Therefore, it is important to know how the rates of carrier generation and recombination are affected by various physical factors involved in PID solar cells.

It is well established that the open-circuit voltage (V_{oc}) and fill factor (FF) are primarily affected by PID in single-crystalline Si (sc-Si) PV modules. It has been reported that the primary limiting factor for V_{oc} in a sc-Si solar cell is bulk recombination in the base.[7] The cell performance depends on the surface recombination velocity (SRV) as well, since an increase in the SRV increases the ideality factor; hence, FF accordingly decreases.[8,9] In PID, the Na ions that reach the Si surface and/or enter the bulk through stacking faults under high potential stress[6,10] increase the defect states in these regions. In addition, free carriers are recombined and/or trapped in these defect states, seemingly reducing FF and V_{oc}. Therefore, we believe that the understanding of the defect states and carrier dynamics in PID cells would be indispensable for elucidating the PID mechanism. In this article, we report the carrier generation and recombination dynamics in fresh and PID-acceleration-tested sc-Si (p-type) PV modules by transient diffuse reflectance spectroscopy (TDRS).

TDRS is a powerful tool used for observing the aforementioned fundamental processes in PV devices directly. It should be noted that the carrier lifetime in Si is a function of the photogenerated carrier density, and various recombination mechanisms could be dominant in different excitation ranges.[11] As described by the Shockley-Read-Hall (SRH) theory, Auger recombination is dominant at a high doping concentration and a high photocarrier generation rate, whereas recombination via impurity or defect states is dominant at a low photocarrier generation rate.[12] Besides, if the carrier lifetime is used to distinguish device characteristics, the recombination around the junction of devices or interfaces including front surface should be considered, because recombination may severely affect the measured lifetime as a result of carrier diffusion. Considering these facts, two different pump wavelengths with various pump fluences have been employed to distinguish device characteristics in terms of carrier lifetime. Recently, carrier dynamics have been studied in polymer-based thin-film solar cells,[13] quantum-dot-sensitized solar cells,[14] FeS_2 solar cells,[15] CdS/CdTe thin films,[16] and GaN/AlN/Si thin films.[17] These studies inspired the present study to further investigate sc-Si PV modules in fresh and PID modes. We examined the dependence of photocarrier dynamics on pump wavelengths at 532 and 1064 nm as well as pump fluences ranging from 0.05 to 4.0 mJ/cm^2. The transient diffuse reflectivity (ΔA) signal showed multiple relaxation components, suggesting the complex behavior of carrier dynamics. For a specific experimental area, carrier dynamics depended on the limit of PID-induced defects.

2 | METHODOLOGY

The sc-Si PV modules were laminated with conventional soda-lime cover glass, commercially available sc-p-type Si PV cells (cell size: 156 × 156 mm^2, efficiency: approximately 17.5%), ethylene vinyl acetate (EVA), and a back sheet. PID was provoked by biasing the modules at −1000 V with respect to their frames in a climate chamber at a temperature of 85°C and relative humidity of 85% for 100 and 300 hours. EL images were taken in forward bias with a current of 40 mA/cm^2 using an InGaAs camera, cooled at around 230 K (Xeva-2.5-320; Xenics Inc., Leuven, Belgium). The local EL intensity was measured using Hokawo 2.1 image analysis software. LIT images were taken by an InGaAs camera, cooled at around 200 K, using a THEMOS-1100L system (Hamamatsu Photonics K.K., Shizuoka, Japan). The light and dark *I-V* curves were recorded at standard spectral irradiance under the AM1.5G condition. Na ions were detected using a high-angle annular dark-field (HAADF) scanning transmission electron microscopy (STEM) system performed by Torey Research Inc. The external quantum efficiency (EQE) spectra of the modules were measured using CEP-2000 (Bunkoukeiki Co., Ltd., Tokyo, Japan) at room temperature. The system was calibrated by a Si reference cell (S-1337BK), and the QE curve was taken in the range of 300 to 1200 nm, with the effective irradiated area remaining as 2.25 cm^2.

TDRS was employed to investigate the photogenerated carrier dynamics in fresh and PID-tested modules. This technique, where diffuse-reflected light is used for investigation instead of transmitted light, is a powerful method to analyze the dynamics of photoexcited states in optically opaque systems. In TDRS, the transient absorption (TA) intensity can be expressed as ΔA, given by $\Delta A = -\log(R/R_0)$, where R and R_0 represent the intensities of diffuse-reflected probe light with and without pump-light excitation, respectively (Figure 1). TDRS measurements were carried out with an Nd:YAG laser (SL311; Ekspla, Vilnius, Lithuania; wavelength: 1064 nm, pulse width: 150 ps, repetition rate: 10 Hz) as a pump-light source. For pump wavelengths of 532 and 1064 nm, the second-harmonic light (532 nm) and fundamental light (1064 nm) of the Nd:YAG laser were used. A steady-state Xe arc lamp (UXL-OBB-75XE; Unisoku Co., Ltd., Osaka, Japan; 75 W) was used as a probe-light source. The pump and probe light were focused on the sample to be a diameter at around 12 and 6 mm, respectively. The diffuse-reflected probe light from the sample was detected using an InGaAs photodetector (DET20C; Thorlabs, Inc., Newton, NJ, USA) after being broadly monochromatized (1500-1800 nm) with an optical filter. At the probe-light wavelength range below the bandgap (E_g) of Si, the photoinduced signals due to the photogenerated carriers in Si can be detected. The alternating current (AC) signal from the photodetector was amplified with a voltage amplifier (DHPVA-100; FEMTO Messtechnik GmbH, Berlin, Germany) before it was processed and analyzed with a digital oscilloscope (WaveRunner 6200A; LeCroy, Chestnut Ridge, NY, USA). The direct current (DC) offset signal from the photodetector was subtracted separately and monitored using a multimeter. The time resolution of the system was around 40 ns.

3 | RESULTS AND DISCUSSION

Figure 2 shows the EL images of a module prepared using only one single solar cell in a fresh manner and after a 100-hour PID-

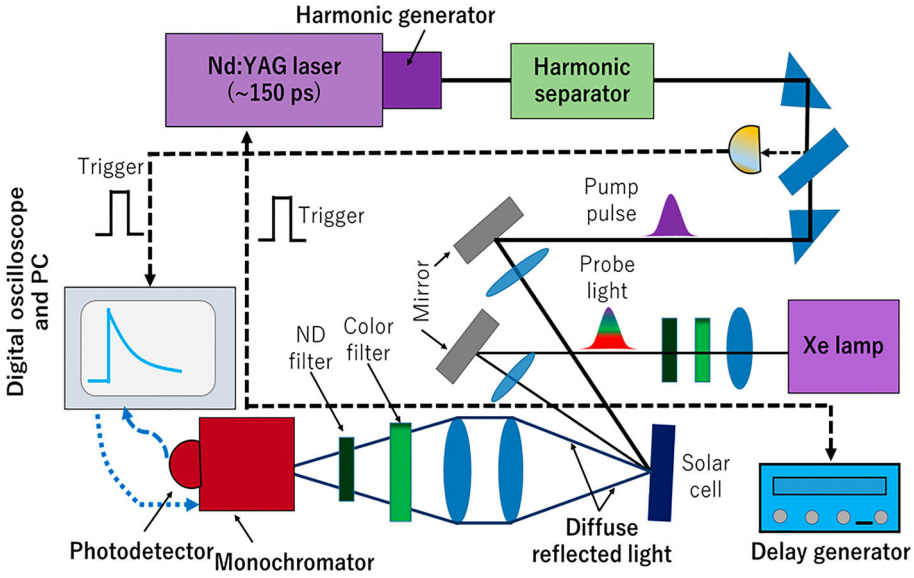

FIGURE 1 Overall schematic illustration of the transient diffuse reflectance spectroscopy (TDRS) measurement setup [Colour figure can be viewed at wileyonlinelibrary.com]

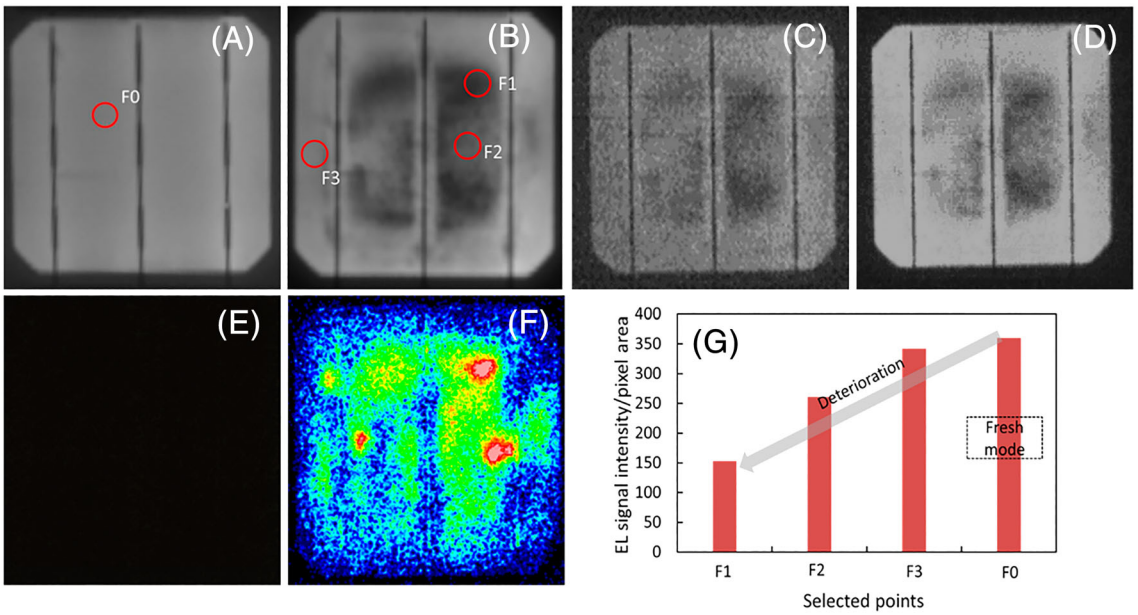

FIGURE 2 Electroluminescence (EL) images of a module (prepared using only one solar cell) A, in a fresh manner and B, after a potential-induced degradation (PID)–acceleration test for 100 hours. C to E show the EL images taken using different spectral filters of C, 1100 ± 25, D, 1200 ± 25, and E, 1600 ± 25 nm, respectively. F, lock-in thermography (LIT) image of the 100-hour PID-acceleration-tested module. G, Comparison of EL images' intensities corresponding to the different selected areas shown in A, and B, [Colour figure can be viewed at wileyonlinelibrary.com]

acceleration test. There was no overilluminated shunt area reported by Wang et al.[18] However, the dark areas in the EL images show that these areas were severely affected by PID. The measured EL intensities for the selected areas, as shown in Figure 2G, gave us a clear indication of the PID effect. The lowest illuminated area, F1, could be considered as the most affected region, where the concentration of Na ions on the SiN_x/Si interface was expected to be maximum. F1 was also found to be the hottest part of the cell in the LIT image (Figure 2F). Therefore, it is assumed that the area of the lowest EL intensity was produced by Na ions–decorated defects.

It is well known that band-to-band luminescence and luminescence from crystal defects (located at around 0.8 eV from the valence band in the polycrystalline Si case) can be observed even at room temperature using the EL technique in forward bias.[19,20] Figure 2C and 2E corresponds to the EL images taken using different spectral filters, such as (C) 1100 ± 25, (D) 1200 ± 25, and (E) 1600 ± 25 nm, with

corresponding energy bands at approximately 1.13, 1.03, and 0.78 eV, respectively. It is clear that no crystal-defect–related EL was detected from the module. Although the emission from the defects was too weak to be detected using an InGaAs camera, it is assumed that the Na migration to the bulk or stacking faults influenced the surface recombination or surface-trap–mediated recombination became dominant. Besides, it could be assumed that the leakage current induced by PID did not occur uniformly (Figure 2B and 2F), suggesting that the Na ions did not migrate uniformly.

In order to confirm the Na diffusion depth and thickness of the Na-induced layer, HAADF-STEM image analyses were conducted on the fresh module and the same batch module after the PID-acceleration test for 300 hours. The experimental figures with the atomic concentration mappings of different elements are shown in Figure 3. In the fresh module, around 2 at.% of oxygen was detected at the Si/SiN_x interface layer. This oxygen may be included during cell fabrication where a thin SiN_xO_y layer (less than or equal to 2 nm) is thermally formed.[21] In the presence of nitrogen and oxygen atoms, the silicon dangling bond defects at the interface were back bonded with Si, N, and O atoms,[22] reducing the defect density. On the other hand, a significant amount of Na was detected at the Si/SiN_xO_y interface in the PID-acceleration–tested modules. Thus, Na-O, Na-N, and Na-Na species were generated at the interface, and they electrically activated the surface in those areas where the Na ions reached the Si surface (the Na ions' layer thickness is around 10 nm in this study) and/or diffused into the Si layer, generating defect states. Dahl et al reported that these types of defects became the acceptor-like state in n-type Si,[23] for which the surface trap center was increased at the Na-migrated regions. Thus, in some areas such as F1 in Figure 2B, where the EL image became the darkest, the defect states were increased if the minority carrier lifetime was reduced drastically.[23] The energy band may have partially changed their electrical behaviors.[24] In addition, another possibility is that while the Na ions reached the Si surface, the induced surface charge concentration was increased as an electrostatic neutrality condition. In this case, depending on the induced negative charge density and the charge carrier density of the n-Si emitter layer, an inverted layer could be formed, where bands change to flat band $p–p^+$ conditions from a rectifying $p–n^+$ junction.[6,25] It should be noted that the space charge that is directly related to the Na ions at the surface needs to be larger than 10^{12} cm^{-2} in order to completely invert the emitter.[26] However, this is beyond the scope of the current work.

Figure 4A and 4B shows the *I-V* characteristics in light and dark conditions of the modules after 100-hour PID-acceleration tests compared with the fresh module. The inset in Figure 4A shows the PV performance. The extensive changes of FF, series resistance (R_s), and shunt resistance (R_{sh}) suggest that the defects were spawned onto the p-n junction and interfaces in some parts of the cell during the PID-acceleration test.[27] It is well known that the most prominent type of defects is the outer edge of an emitter where the p-n junction comes to the surface. In the case of a sc-Si solar cell, this surface is usually a passivation layer using a thin-film oxide or SiN_x as mentioned earlier. For PID, this passivation layer is highly distressed, increasing the defect states by weakening the passivation. Furthermore, the effect of PID was ultimately seen in the dark *I-V* curve, as shown in Figure 4B. The *I-V* curve of the PID-affected modules indicates the

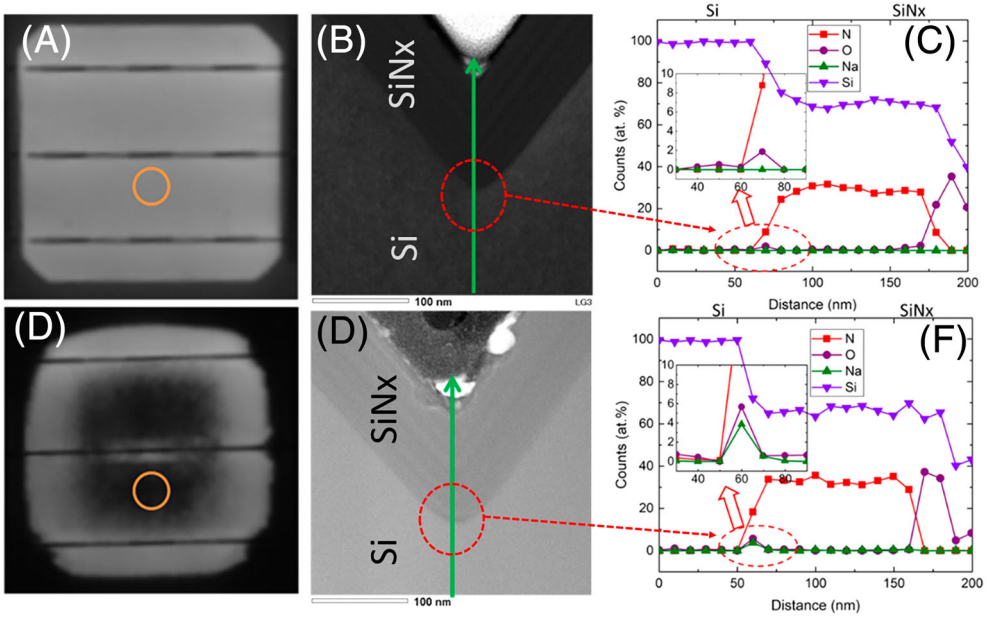

FIGURE 3 A, Electroluminescence (EL) image of a fresh module (circle shows the area selected for high-angle annular dark-field scanning transmission electron microscopy [HAADF-STEM] image analysis), B, and C, show the HAADF-STEM image and the elemental analysis from HAADF-STEM of that fresh module, D, EL image of a 300-hour potential-induced degradation (PID)–acceleration–tested module (circle shows the area selected for HAADF-STEM image analysis), and E, and F, shows the HAADF-STEM image and the elemental analysis from HAADF-STEM of that PID module, arrow sign in B, and E, show the scanning line for elemental analysis and red circles indicate a region at around the interface of Si and SiN_x [Colour figure can be viewed at wileyonlinelibrary.com]

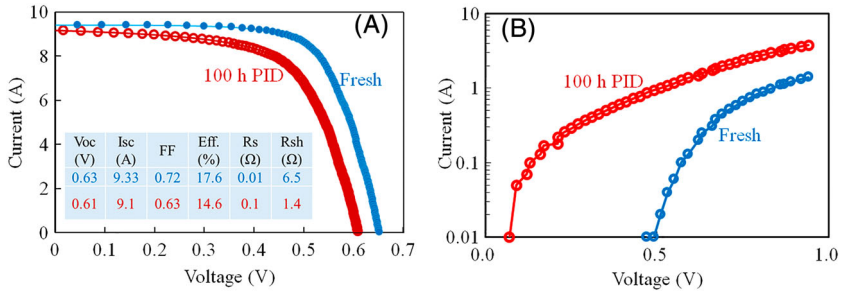

FIGURE 4 A, Comparison of light current-voltage (*I-V*) characteristics of the one-cell module in fresh and 100-hour potential-induced degradation (PID)–acceleration–tested modules and B, comparison of dark *I-V* curves (semi-log scale) of the one-cell module in fresh and 100-hour PID-acceleration-tested modules [Colour figure can be viewed at wileyonlinelibrary.com]

remarkable decrease of shunt resistance and the increase of minority carrier recombination in the depletion regions and the neutral region.

Figure 5 shows the TDRS decay profiles of the fresh and 100-hour PID-acceleration-tested modules for two different pump wavelengths of 532 and 1064 nm. The use of two excitation pump wavelengths allowed us to vary the effective thickness of the excited region, as shown in Figure 5F. Carrier generation and recombination are discussed using the dependence of photocarrier generation on the

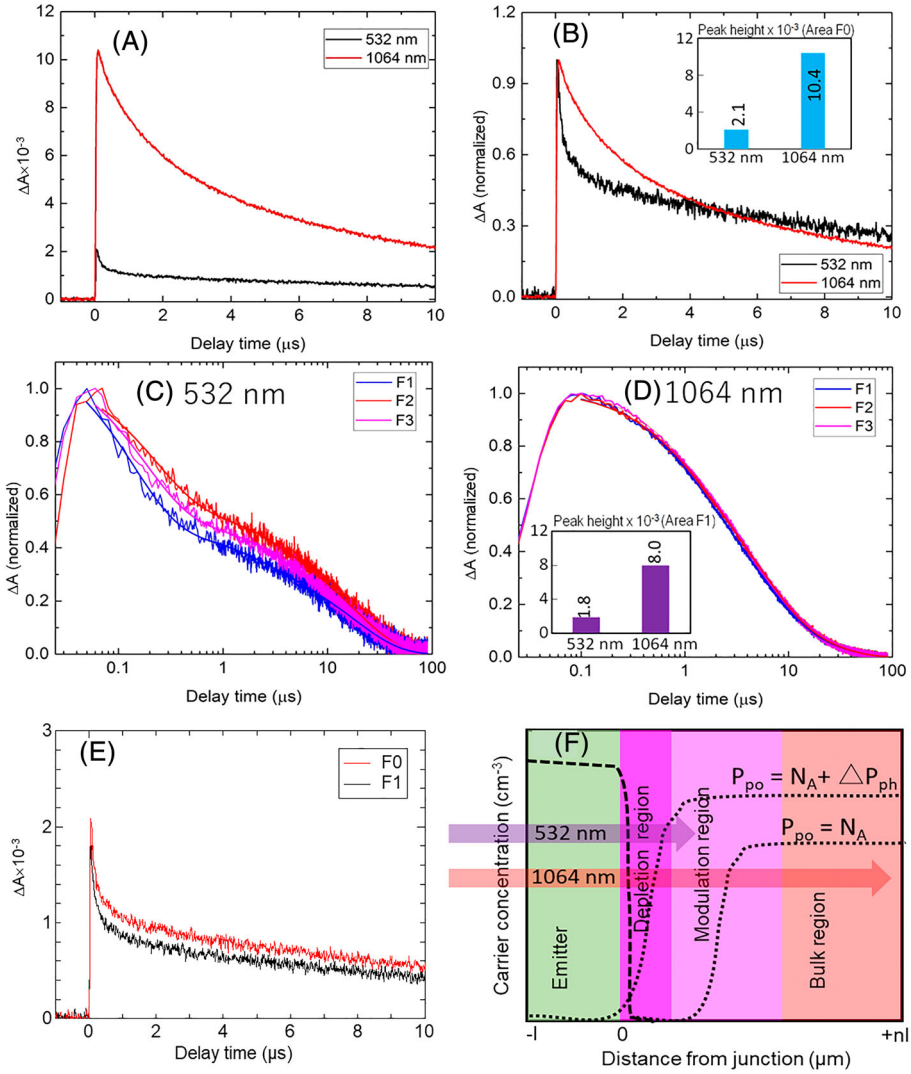

FIGURE 5 A, Transient diffuse reflectance spectroscopy (TDRS) decay spectra of the fresh module at the selected area (F0), as shown in Figure 2 A. B, TDRS spectra of the fresh module in normalized mode. C, D, TDRS decay spectra in semi-log plots of the 100-hour PID-acceleration–tested modules for pump wavelengths of 532 and 1064 nm and a pump fluence of 4.0 mJ/cm^2 (F1, F2, and F3 are the selected areas, as shown in Figure 2B). E, Decay spectra at areas F0 and F1 for the pump wavelength of 532 nm and the pump fluence of 4.0 mJ/cm^2. F, A schematic of the depth profile of the pump pulse, including a simple demonstration of carrier concentrations within the solar cell under pump excitation (three different regions—depletion, modulation, and bulk regions—have been defined considering different carrier concentrations) [Colour figure can be viewed at wileyonlinelibrary.com]

pump fluence as well as the cell condition. As shown in Figure 5F, the TDRS transience of the 1064-nm pump was contributed mainly by the p-Si base including the bulk region. On the contrary, the 532-nm pump had a main contribution from the modulation region of p-Si, but it was significantly influenced by the emitter (n-type Si) interface. It should be noted that the amplitude (max. peak), ΔA, is about four times higher for 1064 nm than for 532 nm for all the ranges of pump fluences (insets of Figure 5B and 5D). In general, ΔA indicates a carrier density that is proportional to the excitation photon number density. Because of the fact that the photon number for the same pump fluence and for the same excitation area for 1064 nm was double that for 532 nm, the number of carriers per unit area was found to be doubled for 1064 nm. Thus, the higher ΔA for 1064 nm than for 532 nm indicates that the different carrier injection properties depended on the depth of the solar cell.

Figure 5A and 5B shows the ΔA decay spectra and the normalized ΔA decay spectra of a module in fresh mode. Figure 5C and 5D shows the normalized ΔA spectra in the semi-log scale for the 100-hour PID-acceleration–tested module for different pump beam wavelengths of 532 and 1064 nm, respectively. In order to understand the deterioration rate that depended on the carrier relaxation through the PID test, the areas were selected according to the EL signal variation, as shown in Figure 2. The typical ΔA curve, as observed in Figure 5, abruptly increased because of the absorption of photon energy above the Si bandgap by photoexcited carriers. The excited photocarriers then sequentially decayed owing to the intraband relaxation, the recombination process, and/or the entrapment at the defect states.[28] The ΔA values of each wavelength for fresh and PID-affected modes at the near-zero delay time are shown in the insets of Figure 5B and 5D. The peak of the spectra indicates the photoexcited carrier density, and the decay curve corresponds to the carrier lifetime that is related to the PV property of a solar cell. A lower ΔA was observed for the PID-acceleration–tested module, suggesting that the photoexcited carrier density in the PID-affected module became lower than that in the fresh module, as also shown in Figure 5E.

It is apparent that the photoexcited carrier density and carrier lifetime were considerably higher for the pump wavelength of 1064 nm, as compared with 532 nm. Alternatively, it was mentioned that the peak height or photoexcited carrier density was also lower for the PID-acceleration-tested module than for the fresh module. These results imply that the density of the defect states in the Si solar cell was differentiated along the depth direction and by the module condition. Considering the penetration depth of the pump beam into the Si solar cell, a wavelength of 532 nm should penetrate only about 1.3 μm, and the 1064-nm pump beam should reach the bulk of the p-type Si base. Therefore, it could be assumed that the charge carriers generated by the 532-nm pump lived for a shorter period than the carriers generated by 1064-nm pump. Such carriers generated by the 532-nm pump received strong effects of surface and bulk defect density. This is also supported by Figure 5C and 5D. Evidently, Figure 5D shows that the spectra were nearly independent of the defect area of the PID-acceleration–tested module. However, the spectra in Figure 5C were varied, indicating that the PID-affected the surface of the solar cell more than the bulk.

Furthermore, Figure 5C and 5D also indicates that the decay profiles had multiple exponential decay functions, implying that the carrier decay occurred by a number of relaxation mechanisms. In order to compare the carrier dynamics, the TDRS decay profiles were fitted (solid line) as triple exponential kinetics using the following equation:

$$y = A_{d1}e^{-x/\tau_1} + A_{d2}e^{-x/\tau_2} + A_{d3}e^{-x/\tau_3}. \quad (2)$$

For comparison, the average decay time constant (τ) was also calculated using the following equation, as reported by Farrow and Kamat[29]:

$$< \tau > = \frac{\sum (A_{di}\tau_i^2)}{\sum (A_{di}\tau_i)}, (i = 1, 2, 3), \quad (3)$$

where A_{di} and τ_i are the triple exponential decay components that indicate the percentage of amplitude and corresponding decay time, respectively. In the measured lifetime, we assume that τ_1 implies the interband relaxation time whereas electrons are relaxed to the valance band via intercenter charge transfer mechanism due to multiple defect levels closely exist within E_g, including surface recombination. In that case, when two or more defect levels are physically close to each other (it could be shallow-deep, shallow-shallow, or deep-deep), electrons are transferred directly between the defects without passing through the bands.[30] This recombination process is very rapid depending on the number of defects[31] and could dominate over the standard SRH recombination process as it is seen in Table 1. However, the assignment of τ_1 still needs a further experiment. On the other hand,

TABLE 1 The estimated τ_1, τ_2, and τ_3 in the 100-hour potential-induced degradation (PID)–acceleration–tested module with respect to the fresh module. The parameters were extracted by the fitting of the transient diffuse reflectance spectroscopy (TDRS) decay profiles of the modules. n = 0, 1, 2, 3

		τ_1 (μs)	τ_{1F0}/τ_{1Fn}	τ_2 (μs)	τ_{2F0}/τ_{2Fn}	τ_3 (μs)	τ_{3F0}/τ_{3Fn}
532 nm	F0	0.21	1.00	8.13	1.00	23.57	1.00
	F1	0.13	0.62	1.28	0.16	16.35	0.69
	F2	0.15	0.71	1.38	0.17	18.16	0.77
	F3	0.15	0.71	1.49	0.18	17.06	0.72
1064 nm	F0	1.23	1.00	6.87	1.00	27.18	1.00
	F1	1.04	0.85	5.16	0.75	20.29	0.75
	F2	1.01	0.82	5.43	0.79	20.62	0.76
	F3	1.06	0.86	5.55	0.81	20.97	0.77

τ_2 and τ_3 correspond to the interband relaxation time either by electron trapping at shallow and deep defect states energetically located within E_g or by the recombination of the electron-hole pair to restore initial states.

As observed in Table 1, τ_1, τ_2, and τ_3 were reduced for the PID-acceleration–tested module in both cases of pump wavelengths of 532 and 1064 nm, indicating that the defects were extended from the surface of the emitter to bulk of the base of the solar cell. The effect for the bulk lifetime, however, was less than that for the surface, as we presumed in the earlier section. In the comparison of the decrement, the values of τ_2 were more reduced compared with the other two for the pump wavelength of 532 nm, indicating that the defect densities were the highest at the shallow level in the PID-acceleration–tested module. The shallow state defects is related to the dislocation where the trapped carrier concentration is varied logarithmically with the trap filling time. Na penetration through stacking faults also affected this decay component. Deep defect states could be introduced as well by dislocation, dangling bond, Na decoration, and contamination by impurities in Si.[32] Thus, as the surface defect density was influenced by Na ions at the emitter surface, the interband recombination states were increased. Consequently, the recombination around the surface was increased, causing the diffused photocarriers to be recombined instantaneously at the traps, especially at the surface,[33] and then to relax to the valence band. This recombination process will relate to τ_1. In the fresh module, τ_2 was governed by the standard SRH recombination. However, in the PID-acceleration–tested module, the electrons were first captured by the shallow state near the conduction band (E_{ST1}) and then immediately transferred to the deep defect center. These transferred electrons were then recombined with a hole captured by the deep center directly or via shallow defects near the valence band (E_{ST2}), while the total recombination process became faster. Similar recombination in Si devices has been reported by Frens et al,[30] Watts et al,[31] and Chen et al.[34] On the other hand, τ_3 is related to a process of direct band-to-band recombination via E_{ST1} or E_{ST2}. The band-to-band recombination via E_{ST1} or E_{ST2} could be explained as a means by which the relaxation time becomes longer than the SRH recombination[35] when no deep defect levels are present and an electron is trapped by E_{ST1}. It should be mentioned that surface recombination is conceptually identical to SRH recombination.[32] Charges like Na ions at the surface may introduce band bending and defect levels at different electronic levels in the forbidden bandgap and complicate the interpretation of the experimental results. Much more investigations are thus needed.

If we compared the values of 532 and 1064 nm, as shown in Table 1, it is clear that the photocarrier generated by 532 nm lived shorter than that generated by 1064 nm, suggesting that the defect density was higher near the surface than that in the bulk. On the other hand, the value of τ calculated by Equation (3) for the 532-nm pump was reduced from 19.8 (fresh) to 15.7 μs (PID-acceleration test for 100 hours). It is readily apparent that the carrier recombination in the n-Si interface was substantially increased by increasing the concentration of Na ions, which is responsible for the low FF in PID-affected modules.[5,10,20] Moreover, by comparing the maximum peak height of the fresh and 100-hour PID-acceleration–tested modules, the areas F1 and F2 were the very low-illuminated regions in the EL image (Figure 2). These points also presented a low peak height, indicating the reduction of charge generation efficiency at these sites. Compared with the values of F0, the local effect of PID was seen in the module, and the combined effect of this local area deterioration was ultimately seen in the cell performance.

Finally, the TDRS transient decay profiles from fresh (F0) and PID (F1) modules at the 532- and 106-nm pump with different pump fluences ranging from 0.05 to 4.0 mJ/cm^2 are shown in Figure 6A and 6B. Figure 6C shows the photocarrier concentration dependence characteristics. It can be seen that the ΔA values increased linearly while maintaining a constant slope of 1.0 by increasing the pump fluence in the case of pump wavelength of 1064 nm. Conversely, the slope of ΔA changed from 1 to 0.5 near the 0.4-mJ/cm^2 fluence of the pump wavelength at 532 nm. Since the pump pulse at 532 nm possessed an energy of 2.33 eV that is higher than the Si indirect bandgap (E_g = ~1.12 eV), the excess energy of conduction band carriers in a solar cell was thermalized through electron-electron or electron-phonon scattering.[36] The initial fast carrier-carrier scattering process beyond the probe time resolution of TDRS (approximately 40 ns) led to nonradiative carrier recombination and suppressed the increase of ΔA at a high pump fluence. Alternatively, the meaning of this deviation may also be related to the increase of trap-assisted Auger recombination, where carriers scattered off the surface are dominant if the photocarrier density exceeds a certain limit near the surface and/or p-n junction. It has also been reported that Auger recombination near the surface occurred twice faster than that in the bulk. Auger recombination is dominant when the excited carrier density is high enough[37] (greater than or equal to 10^{19} cm^{-3}). The ΔA values were thus varied differently after a certain value of pump fluence.

Figure 7 shows the carrier lifetime (τ, estimated using Equation 3) dependence on the 532-nm pump fluence with different carrier excitation densities and depths. It can be seen that, for the pump of 532 nm, the fresh module showed an almost fluence-independent feature, where the PID-acceleration–tested module showed an increasing trend with respect to the pump fluence. τ of F1 did not reach the fresh module level. As 532 nm generated electrons above E_g of Si near the p-n junction (the penetration depth for 532 nm is around 1.3 μm), the photogenerated electrons were immediately captured by the surface and shallow defects. When the surface and shallow-level traps were saturated by carriers via a high pump fluence, the available trap density for the carriers to be captured was reduced. Then, the carrier relaxed through the bulk, like indirect recombination or band-to-band recombination, which is the cause of the slow relaxation by increasing the pump fluence.[38] In the case of the fresh module, the trap density was low enough to saturate even though the fluence was 0.05 mJ/cm^2 for the 532-nm pump. No impact on τ was thus shown. Conversely, the defects at the surface and shallow levels were very high in the PID-acceleration–tested module, and insufficient carriers were generated by the pump fluence to become saturated. However, the number of trapped electrons increased by increasing the photogenerated

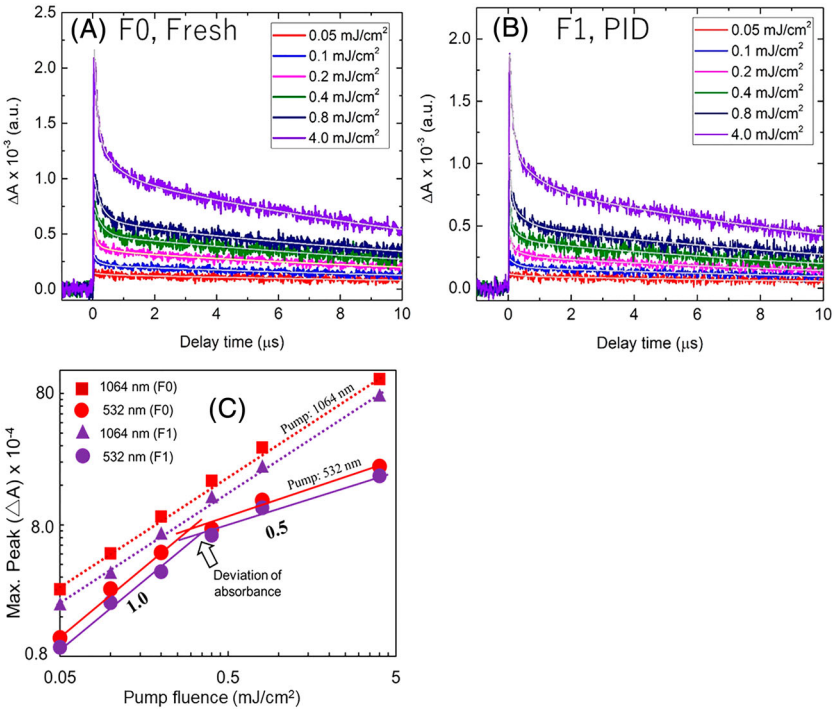

FIGURE 6 A, B, Transient diffuse reflectance spectroscopy (TDRS) carrier transient decay profiles for the 532-nm pump with fluences ranging from 0.05 to 4.0 mJ/cm^2 for fresh and 100-hour potential-induced degradation (PID)–acceleration–tested modules. C, Change of the maximum peak height with respect to the pump fluence for two different pump wavelengths of 532 and 1064 nm. [Colour figure can be viewed at wileyonlinelibrary.com]

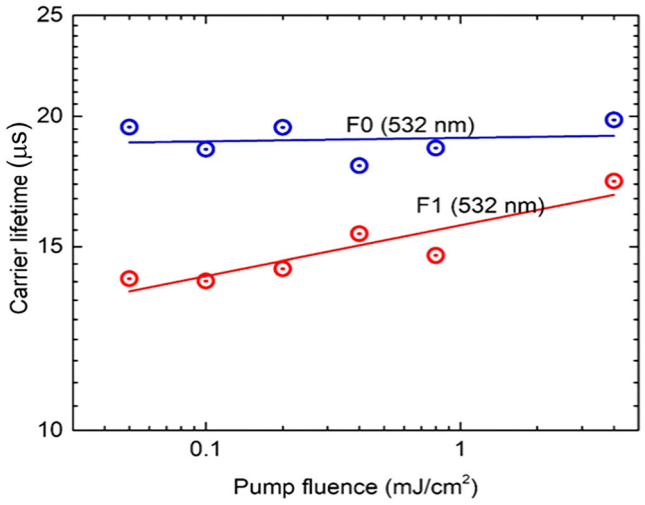

FIGURE 7 Carrier lifetime (τ) for the pump pulse of 532 nm with different pump fluences [Colour figure can be viewed at wileyonlinelibrary.com]

electrons at the conduction band. Thus, τ of F1 showed an increasing trend. It is also mentioned that τ was lower for the PID-acceleration–tested module than for the fresh module all over the range, also indicating the influence of the Auger recombination process. It should be noted that the carrier-carrier Auger recombination must occur in the fresh module as well, as seen in the deviation of ΔA for the 532-nm pump (Figure 6C). However, τ exhibited an almost pump-fluence–independent feature, implying that the fluence-dependent Auger recombination somehow counterbalanced the increase of τ in the fresh mode.

Figure 8A and 8B shows the TDRS decay spectra for the 1064-nm pump with different pump fluences ranging from 0.05 to 4.0 mJ/cm^2 for fresh (F0) and 100-hour PID-acceleration–tested (F1) modules. The fresh module attained a higher peak intensity for the corresponding pump fluence, as can be seen in Figure 8A and 8B. It should be noted that the TDRS spectra for the pump wavelength of 1064 nm showed distinct features depending on the pump fluence; that is, the fluence of 0.05 to 0.1 mJ/cm^2 showed a single exponential fit, the one of 0.2 to 0.8 mJ/cm^2 showed a biexponential fit, and the one of 4.0 mJ/cm^2 showed a triexponential fit for both fresh and PID-acceleration–tested modules. Figure 8C shows the variation of the decay components τ_2 and τ_3 for the pump wavelength of 1064 nm with different fluences. Both decay components in the PID-acceleration–tested module showed faster recombination compared with the fresh module, confirming that the defect extended to the bulk, which may be influenced by the surface deterioration. The mechanism of Na penetration through stacking faults is, thus, supported. For the fresh module, τ_2 and τ_3 showed almost constant behaviors. However, the reducing tendency for τ_2 was presented in the PID-acceleration–tested module (F1), indicating that the inherent defect in the bulk was generated during the PID-acceleration test.

On the other hand, if the electrons are recombined to holes at the valance band via multiple trapping and/or the trap-filled recombination is dominant in solar cells, only the radiative bimolecular band-to-band recombination then becomes increasingly relevant to the EL image. If we consider the mechanism from the EL images of PID-affected cells, it is clear that the band-to-band recombination is dominant at the illuminated areas, whereas the trap-assisted recombination is dominant in the dark areas. However, the trap-filled nonradiative band-to-band recombination would possibly occur partially in both types (fresh and PID) of solar cells. It was reported that the nonradiative band-to-band recombination process via multiple trapping in Si and Si derivative materials occurred at the microsecond

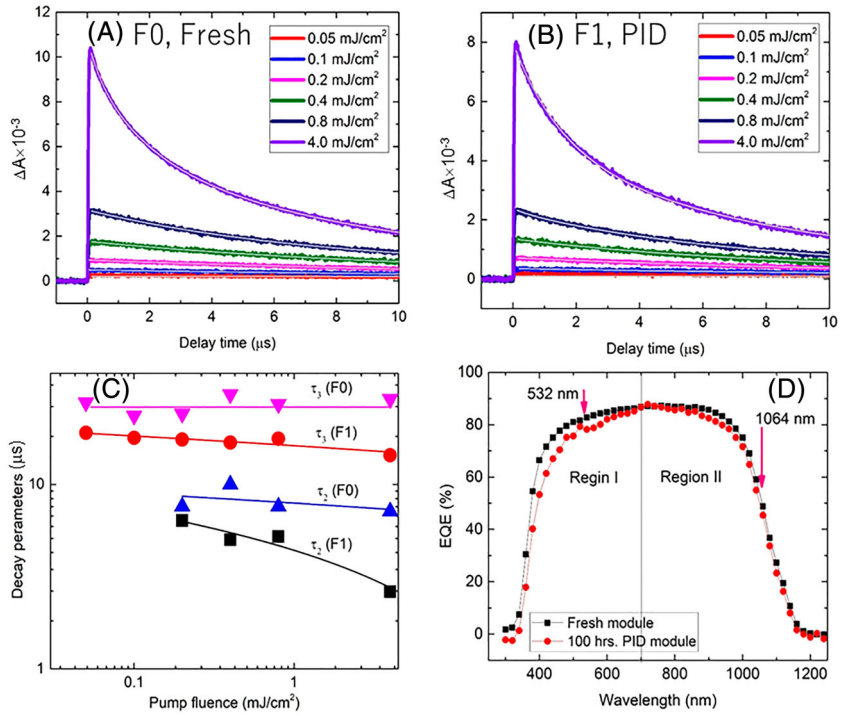

FIGURE 8 A, and B, show the transient diffuse reflectance spectroscopy (TDRS) decay spectra for the pump wavelength of 1064 nm with different pump fluences ranging from 0.05 to 4.0 mJ/cm^2 for fresh (F0) and 100-hour potential-induced degradation (PID)–acceleration–tested (F1) modules. C, Variation of decay components τ_2 and τ_3 with respect to the pump fluence extracted from A, and B. D, External quantum efficiency (EQE) of the fresh and PID-acceleration–tested modules. [Colour figure can be viewed at wileyonlinelibrary.com]

timescale,[39] which is related to τ_2 in the PID-acceleration–tested module. The electron-hole pairs generated at the p-n junction as induced by incident light can reach the interface before they recombine to the ground state and contribute only to solar cell efficiency.[27] Therefore, any interruption during charge transport reduces the efficiency. Here, it is assumed that the Na ions accumulated layer interrupted the SiN_xO_y/Si interfaces by forming Na-O, Na-N, and Na-Na species. In this case, the surface defects were increased and extended from shallow to deep levels, for which the recombination at this stage was increased, consequently reducing the charge collection efficiency. Moreover, the presence of Na ions at the interface of the emitter may reduce its n-type conductivity and shift the Fermi level to the valence band. All of these factors are the causes of free carriers missing at the surface and interfaces, which reduces the carrier collection efficiency and photoconversion efficiency as well.

Finally, from the comparison of the TDRS data analysis using two different pump wavelengths and different pump fluences for fresh and PID-acceleration–tested modules, a clear indication was found for the degradation of the front surface. The results were well supported by the EQE measurement, as shown in Figure 8D. It is well known that the EQE curve can be divided into two regions, where Region 1 (300-600 nm) is greatly dependent on carrier generation, transport, and recombination near the p-n junction region, whereas Region 2 (600 nm and above) corresponds to the effective transport of photogenerated carriers at the bulk and back contact of solar cells.[40,41] The EQE in Region 1 was reduced for the PID-affected module owing to the elevation of carrier recombination at the front side of the solar cell dominated by surface defects. On the other hand, the increases of carrier recombination at the bulk of p-type Si base due to the increase of uncompensated Si bonds influenced by PID in the devices may be the root causes for the decrease of EQEs in Region 2. However, it could be seen that the decrease rate of EQE in the Region 2 is lower than the Region 1. Also it is seen in Figure 8A and 8B that the peak height is about to 20% lower for F1 than F0 for 1064 nm of pump fluence, but EQE did not reduce as well. The cause may be explained from the values of τ_2 and τ_3 as shown in Table 1. It is clearly seen in Table 1 that the values of τ_2 and τ_3 for the pump fluence of 532 nm have reduced much more than those of 1064 nm as compared with the fresh module, suggesting Region 1 has more deteriorated region. The τ_2 and τ_3 for 1064-nm pump fluence also, however, include that deteriorated region (Region 1) as well, leading to providing lower peak height in F1 than the expectation from EQE behavior. Also, another cause may be the back contact that was not qualitatively decreased under the PID stress for which EQE was not decreasing much more for the PID module in the Region 2.

4 | CONCLUSION

The trap limiting carrier dynamics in fresh and PID-acceleration–tested modules were investigated in terms of carrier lifetime, photocarrier density, and different recombination mechanisms using two different pump wavelengths of 532 and 1064 nm as well as pump fluences of 0.05 to 4.0 mJ/cm^2. PID did not occur uniformly over the cell surface, and obviously the photogenerated carrier density and carrier lifetime were found to be weakly dependent on the defect density, as depicted in the EL and LIT image analyses. As a result, the charge collection efficiency, as well as FF and V_{oc}, was reduced in PID-affected modules. The HAADF-STEM image shows that the Na-accumulated layer with a thickness of around 10 nm was generated in the 300-hour PID-acceleration–tested module, inferring that this layer was composed of Na-O, Na-N, and Na-Na species. TDRS decay components show

that the PID-affected module tended to contain shallow-level defects, and the recombination in PID-affected modules occurred via multiple trapping, instead of the standard SRH recombination, leading to short carrier lifetime. The emitter region was highly distressed by PID. However, the defect induced by the PID was extended to the bulk state of the cell, reducing the cell's electrical parameters in the long-wavelength region as well. From the variation of ΔA for the 532-nm pump, the trap-mediated Auger recombination seemed to be dominant at the front side of the cell under a high pump fluence. It was found that the PID defect level could be predicted by TDRS spectroscopy because the carrier lifetime, photogenerated carrier density, and dynamics were found to strongly depend on the cell conditions as well as the depth of light penetration.

ACKNOWLEDGEMENT

This work was supported by the New Energy and Industrial Technology Development Organization (NEDO), Japan.

ORCID

Mohammad Aminul Islam https://orcid.org/0000-0002-3862-9125
Hiroyuki Matsuzaki https://orcid.org/0000-0002-3259-0266
Yasuaki Ishikawa https://orcid.org/0000-0003-4613-6117

REFERENCES

1. Spataru SV, Sera D, Hacke P, Kerekes T, Teodorescu R. Fault identification in crystalline silicon PV modules by complementary analysis of the light and dark current-voltage characteristics. *Prog Photovolt Res Appl*. 2016;24(4):517-532.
2. Hacke P, Smith R, Terwilliger K, Glick S, Jordan D, Johnston S. Testing and analysis for lifetime prediction of crystalline silicon PV modules undergoing degradation by system voltage stress. *IEEE J Photovolt*. 2012;3:246-253.
3. Liu HC, Lee WK, Lin MH, Huang CT, Lin FM, Huang JL. Proc. SPIE 8825, reliability of photovoltaic cells, modules. *Comput Syst*. 2013; VI:88250R.
4. Schütze M, Junghänel M, Köntopp MB, Cwikla S, Friedrich S, Müller JW, Wawer P. Proc. 37th IEEE Photovoltaic Specialists Conference, Seattle, WA, 2011, 000821–000826.
5. Bauer J, Naumann V, Grober S, Hagendorf C, Schütze M, Breitenstein O. On the mechanism of potential-induced degradation in crystalline silicon solar cells. *Phys Status Solidi (RRL)*. 2012;6:331-333.
6. Naumann V, Lausch D, Großer S, et al. Microstructural analysis of crystal defects leading to potential-induced degradation (PID) of Si solar cells. *Energy Procedia*. 2013;33:76-83.
7. Aberle AG, Altermatt P, Heiser G, et al. Limiting loss mechanisms in 23% efficient silicon solar cells. *J Appl Phys*. 1995;77(7):3491-3504.
8. Aberle AG, Robinson S, Wang A, Zhao J, Wenham SR, Green MA. High-efficiency silicon solar cells: full factor limitations and non-ideal diode behaviour due to voltage-dependent rear surface recombination velocity. *Prog Photovolt Res Appl*. 1993;1(2):133-143.
9. Robinson S, Aberle AG, Green MA. Recombination saturation effects in silicon solar cells. *IEEE Trans Elec Devices*. 1994;41(9):1556-1569.
10. Naumann V, Lausch D, Hähne A, et al. Explanation of potential-induced degradation of the shunting type by Na decoration of stacking faults in Si solar cells. *Sol Energy Mater Sol Cells*. 2014;120:383-389.
11. Linnros J. Carrier lifetime measurements using free carrier absorption transients. I. Principle and injection dependence. *J Appl Phys*. 1998;84(1):275-285.
12. Shockley W, Read WT. Statistics of the recombinations of holes and electrons. *Phys Rev*. 1952;87(5):835-842.
13. Ohkita H, Ito S. Transient absorption spectroscopy of polymer-based thin-film solar cells. *Polymer*. 2011;52(20):4397-4417.
14. Lee J-W, Son D-Y, Ahn TK, et al. Quantum-dot-sensitized solar cell with unprecedentedly high photocurrent. *Sci Rep*. 2013;1050(1–8):3.
15. Shukla S, Xing G, Ge H, et al. Origin of photocarrier losses in iron pyrite (FeS2) nanocubes. *ACS Nano*. 2016;10(4):4431-4440.
16. Pandit B, Dharmadasa R, Dharmadasa IM, Druffel T, Liu J. Ultrafast charge carrier relaxation and charge transfer processes in CdS/CdTe thin films. *Phys Chem Chem Phys*. 2015;17(26):16760-16766.
17. Dugar P, Kumar M, Krishna TCS, Aggarwal N, Gupta G. Carrier relaxation dynamics in defect states of epitaxial GaN/AlN/Si using ultrafast transient absorption spectroscopy. *RSC Adv*. 2015;5(102):83969-83975.
18. Wang E, Yang HE, Yen J, Chia S, Wang C. Failure modes evaluation of PV module via materials degradation approach. *Energy Procedia*. 2013;33:256-264.
19. Bothe K, Ramspeck K, Hinken D, et al. Luminescence emission from forward- and reverse-biased multicrystalline silicon solar cells. *J Appl Phys*. 2009;106(10):104510.
20. Islam MA, Oshima T, Kobayashi D, Matsuzaki H, Nakahama H, Ishikawa Y. Carrier dynamics in the potential-induced degradation in single-crystalline silicon photovoltaic modules. *Jpn J Appl Phys*. 2018;57(8S3):08RG14.
21. Elmiger JR, Kunst M. Investigation of the silicon-plasma silicon nitride interface with in situ transient photoconductivity measurements. *Appl Surf Sci*. 1996;103(1):11-18.
22. Schmidt J, Aberle AG. Carrier recombination at silicon–silicon nitride interfaces fabricated by plasma-enhanced chemical vapor deposition. *J Appl Phys*. 1999;85(7):3626-3633.
23. Dahl EH, Madsbøll J, Søiland A-K, Odden J-O, Tronstad R, Larsen AN. Electrically active sodium-related defect centres in silicon. *Semicond Sci Technol*. 2013;28(10):105010.
24. Pingel S, Frank O, Winkler M, Daryan S, Geipel T, Hoehne H, Berghold J. Proc. 35th IEEE Photovoltaic Specialists Conference, Honolulu, HI, 2010, 002817–002822.
25. Bauer J, Naumann V, Großer S, Hagendorf C, Schütze M, Breitenstein O. On the mechanism of potential-induced degradation in crystalline silicon solar cells. *Phys Status Solidi (RRL)*. 2012;6(8):331-333.
26. Saint-Cast P, Nagel H, Wagenmann D, Schön J, Schmitt P, Reichel C, Glunz SW, Hofmann M, Rentsch J, Preu R, Proc. 28th Eur Photovoltaic sol Energy Conf Exhib, 2013, 789–792.
27. Macdonald D, Cuevas As. *Prog Photovolt Res Appl*. 1999;7:252-264.
28. Ulbricht R, Hendry E, Shan J, Heinz TF, Bonn M. Carrier dynamics in semiconductors studied with time-resolved terahertz spectroscopy. *Rev Mod Phys*. 2011;83(2):543-586.
29. Farrow B, Kamat PV. CdSe quantum dot sensitized solar cells. Shuttling electrons through stacked carbon nanocups. *J Am Chem Soc*. 2009;131(31):11124-11131.
30. Frens AM, Bennebroek MT, Zakrzewski A, et al. Observation of rapid direct charge transfer between deep defects in silicon. *Phys Rev Lett*. 1994;72(18):2939-2942.
31. Watts SJ, Matheson J, Hopkins-Bond IH, Holmes-Siedle A, Mohamadzadeh A, Pace R. A new model for generation-recombination in silicon depletion regions after neutron irradiation. *IEEE Trans Nucl Sci*. 1996;43(6):2587-2594.

32. Wong J, Huang JL, Eggleston B, et al. Lifetime limiting recombination pathway in thin-film polycrystalline silicon on glass solar cells. *J Appl Phys*. 2010;107:123705(1)-123705(7).

33. Schroder DK. *Semiconductor Material and Device Characterization*. New York: Wiley; 1990:359.

34. Chen WM, Monemar B, Janzén E. Direct observation of intercenter charge transfer in dominant nonradiative recombination channels in silicon. *Phys Rev Lett*. 1991;67(14):1914-1917.

35. Norton P, Braggins T, Levinstein H. Recombination of electrons at ionized donors in silicon at low temperatures. *Phys Rev Lett*. 1973;30(11):488-489.

36. In C, Seo J, Kwon H, et al. Counterbalanced effect of surface trap and Auger recombination on the transverse terahertz carrier dynamics in silicon nanowires. *IEEE Trans Tera Sci Tech*. 2015;5(4):605-612.

37. Tanaka T, Harata A, Sawada T. Imagings of picosecond-photoexcited carriers and enhanced Auger recombination rate by transient reflecting grating measurements, part 1. *Jpn J Appl Phys*. 1996;35(6A):3642-3647.

38. Uhd Jepsen P, Schairer W, Libon IH, et al. Ultrafast carrier trapping in microcrystalline silicon observed in optical pump–terahertz probe measurements. *Appl Phys Lett*. 2001;79(9):1291-1293.

39. He W, Zakar A, Roger T, Yurkevich IV, Kaplan A. Determination of recombination coefficients for nanocrystalline silicon embedded in hydrogenated amorphous silicon. *Opt Lett*. 2015;40(16):3889-3892.

40. Islam MA, Rahman KS, Sobayel K, et al. Fabrication of high efficiency sputtered CdS:O/CdTe thin film solar cells from window/absorber layer growth optimization in magnetron sputtering. *Sol Energy Mater Sol Cells*. 2017;172:384-393.

41. Tsui K-H, Lin Q, Chou H, et al. Low-cost, flexible, and self-cleaning 3D nanocone anti-reflection films for high-efficiency photovoltaics. *Adv Mater*. 2014;26(18):2805-2811.

How to cite this article: Aminul Islam M, Matsuzaki H, Okabayashi Y, Ishikawa Y. Transient carrier recombination dynamics in potential-induced degradation p-type single-crystalline Si photovoltaic modules. *Prog Photovolt Res Appl*. 2019;27:682–692. https://doi.org/10.1002/pip.3143